THE JOURNAL OF PHYSICAL CHEMISTRY C

Article

pubs.acs.org/JPCC

Confirmation of Isolated Cu^{2+} Ions in SSZ-13 Zeolite as Active Sites in NH_3-Selective Catalytic Reduction

Upakul Deka,[†,‡] Amélie Juhin,[§] Einar A. Eilertsen,[∥] Hermann Emerich,[⊥] Mark A. Green,[⊗,○] Satu T. Korhonen,[‡] Bert M. Weckhuysen,[‡] and Andrew M. Beale*[,‡]

[†]Materials Innovation Institute (M2i), Mekelweg 2, 2628 CD Delft, The Netherlands

[‡]Inorganic Chemistry and Catalysis Group, Debye Institute of Nanomaterials Science, Utrecht University, Universiteitsweg 99, 3584 CA Utrecht, The Netherlands

[§]Institut de Minéralogie et de Physique des Milieux Condensés, CNRS, Université Pierre et Marie Curie, Case courier 115, 4 place Jussieu 75252, Paris Cedex 05, France

[∥]SMN/INGAP/Department of Chemistry, University of Oslo, Sem Selands vei 26, 0315 Oslo, Norway

[⊥]Swiss Norwegian Beamline (SNBL, BM01), ESRF, BP 220, F-38043 Grenoble, France

[⊗]Beamline BT1, NIST Center for Neutron Research, National Institute of Standards and Technology, 100 Bureau Drive, Gaithersburg, Maryland 20878, United States

[○]Department of Materials Science and Engineering, University of Maryland, College Park, Maryland 20742, United States

Supporting Information

ABSTRACT: NH_3-Selective Catalytic Reduction (NH_3-SCR) is a widely used technology for NO_x reduction in the emission control systems of heavy duty diesel vehicles. Copper-based ion exchanged zeolites and in particular Cu-SSZ-13 (CHA framework) catalysts show both exceptional activity and hydrothermal stability for this reaction. In this work, we have studied the origin of the SCR activity of Cu-SSZ-13 as evidenced from a combination of synchrotron-based and laboratory techniques. Synchrotron-based in situ XAFS/XRD measurements were used to provide complementary information on the local copper environment under realistic NH_3-SCR conditions. Crucial then to the catalytic activity of Cu-SSZ-13 is the local environment of the copper species, particularly in the zeolite. Cu-SSZ-13 contains mononuclear Cu^{2+} species, located in the face of the double-6-ring subunit of the zeolite after calcination where it remains under reaction conditions. At lower temperatures (with low activity), XAFS and XRD data revealed a conformational change in the local geometry of the copper from a planar form toward a distorted tetrahedron as a result of a preferential interaction with NH_3. This process appears necessary for activity, but results in a stymieing of activity at low temperatures. At higher temperatures, the Cu^{2+} possess a local coordination state akin to that seen after calcination.

INTRODUCTION

Each year, over 30 million tons of anthropogenic nitrogen oxides (NO_x) are released into the earth's atmosphere. A large part of this comes from vehicular transport emissions. As a result, the past two decades have seen a series of legislations introduced in Europe, United States, and Japan limiting the amounts of harmful exhaust gases produced by automobiles. More recent regulations, specifically in diesel emission control, are expected to require as high as 5-fold reduction in the amount of NO_x present in the exhaust.[1,2] This has increased the need to develop new, efficient catalysts with a wide temperature range of activity (especially at lower temperatures) and a high selectivity toward N_2.

Ammonia-Selective Catalytic Reduction (NH_3SCR) is an effective technology for the reduction of NO_x gases in mobile applications. NH_3-SCR typically uses metal-oxides, noble metals, or metal exchanged zeolites as catalysts. However, the drawbacks of noble metals are their high costs and high selectivity toward N_2O.[3] Metal oxides (especially based on vanadium), while being popular for stationary SCR applications, are being phased out in mobile applications in favor of less toxic catalysts. Metal exchanged zeolites are promising catalysts for mobile emission control applications due to their lower price, nontoxicity, and high activity and selectivity to N_2.[4]

In particular, zeolite systems such as Cu-ZSM-5, Fe-ZSM-5, and Fe-beta, were found to be efficient for NH_3-SCR and have received much attention both from academia and industry. However, recent studies have shown that Cu loaded SSZ-13

Received: December 24, 2011
Revised: January 18, 2012
Published: January 24, 2012

   dx.doi.org/10.1021/jp212450d | J. Phys. Chem. C 2012, 116, 4809−4818

zeolites with the chabasite (CHA) structure are very promising catalysts expected to meet with our future needs, especially owing to their low temperature activity and high hydrothermal stability.[5,6] Although several mechanistic and characterization studies have been performed on NH_3-SCR systems, the active sites for this reaction still remain a topic of debate. In the case of copper-based systems active for SCR or NO decomposition, both dimeric Cu species[4,7] and isolated Cu^{2+} ions[8,9] have been proposed as the active sites. From a more mechanistic perspective, the importance of a Cu^{2+}/Cu^{+} redox pair-based mechanism has also been stressed.[10−12] Recently, Fickel et al. were able to successfully show the location of copper ions in the double six member (d6r) ring of the Cu-SSZ-13 structure using Rietveld refinement of X-ray diffraction data.[13] Further catalytic studies combined with in situ UV−vis and ex situ X-ray absorption (XAFS) measurements were performed by Korhonen et al. comparing Cu-ZSM-5 and Cu-SSZ-13 for both SCR and NO decomposition reactions.[14] On the basis of these findings, we proposed that isolated Cu^{2+} ions located in the plane and slightly off the center of the d6r in CHA are active sites for NH_3-SCR.

Despite several mechanistic, kinetic, and spectroscopic studies previously performed, no conclusive evidence of particular active species in copper-zeolites for the NH_3-SCR reaction in operando conditions have been established. In this study, we show for the first time the active copper species in NH_3-SCR under realistic reaction conditions using a combination of synchrotron-based in situ X-ray absorption and diffraction studies.

EXPERIMENTAL SECTION

Catalyst Preparation. SSZ-13 was prepared from an unseeded reaction mixture forming a gel with the following composition: 10 TMAda-OH/5 Na_2O/4 Al_2O_3/100 SiO_2/2200 H_2O. The gel was prepared by first mixing solutions of NaOH (1M, VWR International), TMAda-OH (1M, Sachem ZeoGen 2825), and deionized water. Al_2O_3 (54% hydrate, Aldrich) was then added to the solution and stirred until the powder was dissolved. This mixture was mixed with Cab-O-Sil M5 (Cabot) fumed silica. The resulting viscous gel was homogenized by hand for 5 min and aged at room temperature for 2 h. The gel was then heated statically for 4 days at 160 °C in a 15 mL Teflon-lined steel autoclave. Cu-SSZ-13 was prepared via wet ion exchange of the parent SSZ-13 (0.91 g) with a solution of 0.1 M $CuSO_4$ in 50 mL water. The slurry was continuously stirred for 3 h at 80 °C. The exchanged zeolite was separated using vacuum filtration, dried overnight at 120 °C, and further calcined in air at 500 °C to obtain Cu-SSZ-13. The thus obtained catalyst was found to have a 3.6 wt % of copper as per ICP analysis.

Catalyst Precharacterization. Laboratory-based XRD was collected using a Bruker D8 ADVANCE diffractometer with a Co Kα source. Patterns were obtained from 5−60° 2θ using a step size of 0.017° 2θ and a collection time of 1s per step. Ex situ UV−vis-NIR spectra were collected using Varian Cary 500 UV−vis-NIR spectrometer equipped with a diffuse reflectance spectroscopy (DRS) accessory. Spectra were collected between 5000 and 50 000 cm^{-1} wavenumbers with a data interval of 10 cm^{-1} and at a rate of 6000 cm^{-1}/min.

Catalyst Testing. Catalytic activity tests were performed in an in-house built catalytic rig under plug flow conditions using 200 mg of powdered catalyst (sieve fractions of 0.45−0.125 mm). The catalyst was placed in a quartz tube-reactor inside a ceramic oven (Figure S1, Supporting Information). A feed composition of 1000 ppm NO, 1000 ppm NH_3, and 5% O_2 (with He for balance) was used adding up to a Gas Hourly Space Velocity (GHSV) of 100 000 h^{-1}. All gases were provided by Linde, and the flows were controlled using a set of Brooks 5850 mass flow controllers. To study their activity, Cu-SSZ-13 were precalcined in a 10% O_2/He flow. Following the calcination, samples were heated from 50 to 500 °C at a rate of 5 °C/min, while the output gases were analyzed online by mass spectrometry (MS, Hiden Analytical, HPR-20 QIC), and infrared (IR) spectroscopy (Perkin-Elmer, Spectrum One). A gas cell with KBr windows and a path length of ∼5 cm was used for the IR analysis. The spectra were measured in continuous mode (using Time-Base software by Perkin-Elmer) in the range 4000−700 cm^{-1} with a spectral resolution of 8 cm^{-1} and an acquisition of 40 scans per spectrum, resulting in a time interval of 44 s between each spectrum. Alternatively, Cu-SSZ-13 was also studied under steady-state conditions at 300 °C using the same conditions and instrumentation.

Neutron Scattering. Constant wavelength (CW) neutron scattering measurements were performed at beamline BT1, NIST Center for Neutron Research, Gaithersburg, MD. The experiments were performed at room temperature on a calcined sample using a Ge(311) monochromator yielding neutrons at a wavelength of 2.079 Å. Scattering data were recorded between 3−140 2θ (degrees) using 32 Helium-3 detectors at 5° (2θ) offsets. Rietveld refinement of the scattering data was performed using the GSAS[15] core along with EXPGUI (graphical interface).[16] The initial hexagonal unit cell dimensions ($a = b$ = 13.675 Å; c = 14.767 Å) with a $R\bar{3}m$ space group was taken from the International Zeolite Association (IZA) Web site for the CHA framework.[17] Starting atomic coordinates were taken from the structure by Fickel et al.[13] The background profile was edited manually choosing 22 points over the pattern and further using a 6-term power series function. The peak profiles were modeled using a Pseudo-Voigt function. Only symmetry constraints were used while modeling the position of atoms in the unit cell. All tetrahedral positions were modeled as Si atoms. The thermal parameters (U_{iso}) for all oxygen atoms were grouped during the refinement.

X-ray Absorption near Edge Structure (XANES) Simulations. First-principles Cu K-edge XANES calculations were performed using the QUANTUM-ESPRESSO code based on Density Functional Theory (DFT).[18] The code uses plane waves and periodic boundary conditions. By adopting the general gradient approximation, the simulated XANES spectrum was obtained in two steps: first, the charge density was calculated self-consistently for the structure including the 1s core-hole using the PW package, then the absorption cross-section was computed as a continued fraction using the XSPECTRA package.[19−21] The simulations were based on the structural model as obtained from the EXAFS data using a Cu-SSZ-13 unit cell of 114 atoms. For Cu, Si, and O, we used ultrasoft pseudopotentials. The electronic configurations were, repectively, $3d^{10}$ $4s^1$ $4p^0$ with nonlinear core correction for Cu, $3s^2$ $3p^2$ with nonlinear core correction for Si, and $2s^2$ $2p^4$ for O. The pseudopotential of the Cu absorbing atom was obtained by considering only one 1s electron in the electronic configuration of the copper atom. The absorption cross-section was computed in the electric dipole approximation, and the isotropic XANES spectrum was calculated. Convergence of the XANES spectrum was reached for the following set of parameters: a 35 Ry energy cutoff for the plane-wave expansion,

dx.doi.org/10.1021/jp212450d | J. Phys. Chem. C 2012, 116, 4809−4818

a 1 × 1 × 1 *k*-point grid for the self-consistent charge density calculation, and a 3 × 3 × 3 *k*-point grid for the absorption cross-section calculation. For the convolution of the XANES spectrum, we used a constant broadening parameter of 2.2 eV directly within the continued fraction.

Synchrotron-Based X-ray Absorption Fine Structure/X-ray Diffraction (XAFS/XRD). Combined XAFS/XRD measurements were performed at the Swiss-Norwegian beamline (SNBL; BM01) in the European Synchrotron Research Facility (ESRF), Grenoble, France. Using a Si(111) double crystal monochromator, X-ray absorption data at the Cu K-edge (8979 eV) was collected in transmission mode. X-ray diffraction was recorded between 2−25° 2θ at a wavelength (λ) of 0.50117 Å. This diffractometer features six Si(111) analyzer crystals. The diffracted X-rays for each channel finally get detected by their respective single photon scintillation counters. A schematic of the setup used is illustrated in Figure S1, Supporting Informatin. The collected diffraction data was then summed and averaged over all the detectors. The diffraction and absorption data were collected in rapid succession to each other during all stages of the experiment. The measurements were performed on powdered samples packed (sieve fractions of 90−125 mm) in 2 mm quartz capillaries under flow conditions. A preassembled gas rig at BM01 was used to dose the samples with the required gases at different flow rates. The outlet gases were analyzed by a mass spectrometer (MS) to identify the outlet composition. The samples were calcined at 500 °C in 10% O_2/He prior to being exposed to SCR conditions. The catalysts were then studied under SCR conditions with a feed composition of 1000 ppm NO, 1000 ppm NH_3, 5% O_2, and He for balance making up to a GHSV of 100 000 h^{-1}. Under the mentioned flow conditions, the system was heated to 300 °C with a ramp of 2 °C/min and allowed to dwell at 300 °C for 30 min to reach a steady state.

The X-ray absorption data was background corrected using Athena (IFFEFIT software package). The normalized data was k^3-weighed and a least-squares fitting analysis was performed in a k-range of 2.8 (or 3)−10 $Å^{-1}$. The FT of the k^3-weighed data were phase corrected and fit to the proposed theoretical model using the DL-EXCURV program.[22] Multiple scattering calculations on a defined cluster of 5 Å were performed on the data obtained after calcination. The coordination numbers were fixed, and the Debye−Waller factors were grouped during the fitting. Data collected under SCR conditions were analyzed in the same *k*-range but considering only single scattering paths. An amplitude reduction factor (S_o^2) value of 0.9 was used for all data sets with the *R*-factor being used as a determinant for the best fit. Rietveld refinement of all X-ray diffraction data (2.8−20° 2θ) was performed using the FULLPROF[23] package along with WinPLOTR interface.[24] The initial hexagonal unit cell dimensions ($a = b = 13.675$ Å; $c = 14.767$ Å) with a $R\bar{3}m$ space group was taken from the International Zeolite Association (IZA) Web site for the CHA framework.[17] Starting atomic coordinates were taken from the suggested structure by Fickel et al.[13] The background profile was edited manually by choosing 40 points over the pattern and further using a cubic-spline interpolation. The peak profiles were modeled using a Pseudo-Voigt function, while accounting for asymmetry below 10° 2θ. Only symmetry constraints were used while modeling the position of atoms in the unit cell. All tetrahedral positions were modeled as Si atoms. The thermal parameters (B_{iso}) for all oxygen atoms were grouped during the refinement.

RESULTS AND DISCUSSION

Catalytic Activity Tests. Figure 1I shows the conversion of NO over Cu-SSZ-13 under NH_3-SCR conditions as a function

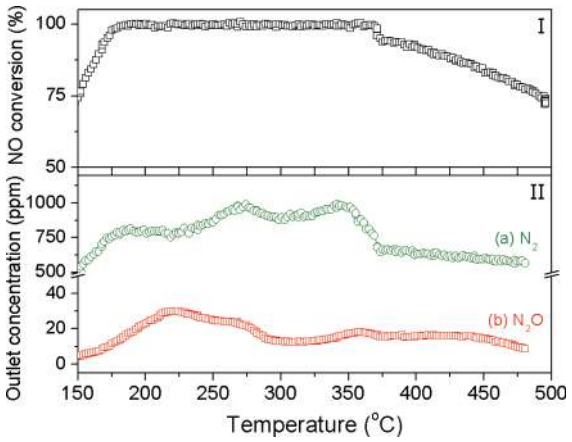

Figure 1. Conversion of (I) NO and (II) formation of (a) N_2 and (b) N_2O as a function of temperature during NH_3-SCR over Cu-SSZ-13. Plug flow conditions: 1000 ppm NO; 1000 ppm NH_3; 5% O_2; GHSV, 100 000 h^{-1}.

of reaction temperature. Additionally, the amounts of N_2 and N_2O formed during the same reaction are plotted in Figure 1II. As can be seen, Cu-SSZ-13 shows remarkable NO_x conversion activity over a wide temperature window (>90% conversion between ∼175−350 °C). The catalyst also shows very high selectivity toward N $_2$, while only small amounts (max 30 ppm at 225 °C) of undesired N_2O is formed over the tested temperature window. Steady-state activity tests were also performed on Cu-SSZ-13 under the same flow conditions at 300 °C, and the results are summarized in Figure 2. Figure 2I

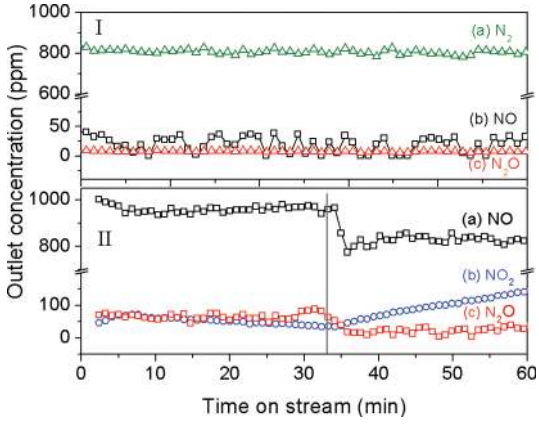

Figure 2. Outlet gas compositions during steady state experiments performed at 300 °C over Cu-SSZ-13. (I) SCR plug flow conditions: 1000 ppm NO; 1000 ppm NH_3; 5% O_2; GHSV, 100 000 h^{-1}. (II) NO decomposition plug flow conditions: 1000 ppm NO; (II, after 30 min) NO oxidation conditions: 1000 ppm NO; 5% O_2.

shows the outlet composition during NH_3-SCR performed over Cu-SSZ-13 at 300 °C. As clearly seen, N_2 is the main product over the tested 60 min with trace amounts of N_2O and NO seen at the outlet. Figure 2II shows the outlet composition upon flowing either NO or NO + O_2 over Cu-SSZ-13. This was performed to test both the NO decomposition and NO oxidation activity of the catalyst material. During the first 30

dx.doi.org/10.1021/jp212450d | J. Phys. Chem. C 2012, 116, 4809−4818

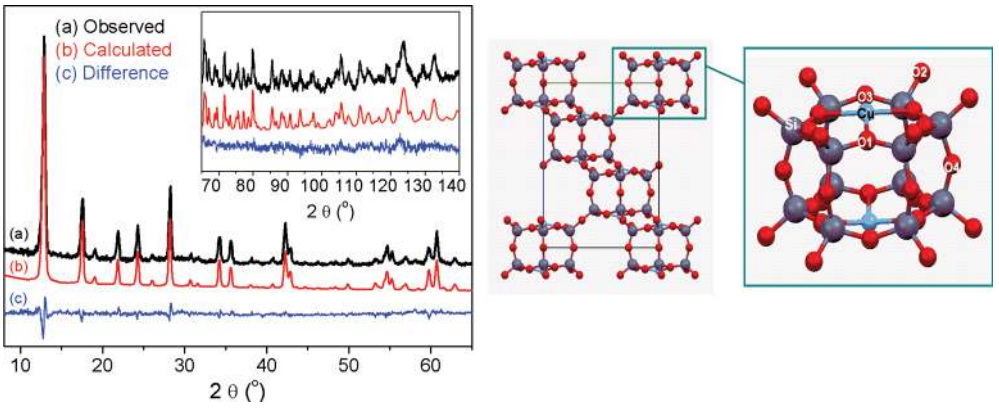

Figure 3. (Left) Observed (black), calculated (red), and difference (blue) patterns obtained from Rietveld refinement of constant wavelength neutron scattering data collected on Cu-SSZ-13 after calcination. (Left inset: magnification of data between 70−140 2 θ). (Right) Corresponding structure of Cu-SSZ-13 obtained from refinements and magnification of the d6r unit with Cu present as an isolated ion. Neutron radiation λ = 2.079 Å; space group, $R\bar{3}m$; refined unit cell, $a = b$ = 13.56 Å, c = 14.77 Å; vol, 2352.61 Å^3.

min, 1000 ppm of NO was flowed over the catalyst. As reported previously,[14] Cu-SSZ-13 shows very poor NO decomposition activity as seen by the large amounts of unreacted NO present in the outlet, while a maximum of ∼75 ppm of N_2O is seen. After 30 min, 5% O_2 was added to the feed. As seen from the outlet composition after ∼35 min, NO oxidizes to form NO_2 with an increasing profile over the course of time. However, no NO_2 is seen at the outlet during SCR conditions. This suggests that any NO_2 that might form in situ with or without the presence of the catalyst would be immediately consumed by the reactants under SCR conditions to form N_2.

Ex Situ Catalyst Characterization. *UV−vis-NIR DRS Spectroscopy and Laboratory-Based Powder X-ray Diffraction.* Figure S2 of the Supporting Information shows the ex situ UV−vis-NIR DRS spectra and powder X-ray diffraction for Cu-SSZ-13 before and after SCR. The UV−vis-NIR DRS spectra show two bands, which are assigned to a Cu^{2+} d−d transition at ∼12 000 cm^1 and a LMCT (O → Cu^{2+}) at ∼47 000 cm^{-1}.[25] Powder X-ray diffraction patterns were also collected on Cu-SSZ-13 before and after SCR. The identical peak positions and background suggests no loss in crystallinity of the zeolite and no visible formation of either metallic or oxidic copper.

Neutron Scattering Analysis. Figure 3 shows the measured and refined pattern along with the difference curve from a neutron scattering analysis. As seen from the difference curve, the refinement agrees well with the experimental pattern. Experimental parameters and conventional goodness of fit parameters for rietveld refinements are shown in Table 1. The

Table 1. Experimental Parameters and Goodness of Fit Factors Obtained from Rietveld Refinement of CW-Neutron Scattering Data Obtained on Cu-SSZ-13 after Calcination

exp parameter	value	refinement parameter	value
wavelength (λ)	2.079 Å	χ^2	1.6
scanned region (2θ)	3−150	R_{wp}	5.76
refinement region (2θ)	3−140	R_p	4.92

low R_{wp} value of 5.76 (0.0576 in GSAS) and a χ^2 value of 1.6 both together indicate a very good agreement with the experimental data. Table 2 lists the refined atom positions, thermal parameters, and fractional occupancies of the Cu-SSZ-13 unit cell ($R\bar{3}m$) with dimensions of $a = b$ = 13.349 Å, c = 14.803 Å, and volume = 2351.925 Å^3. Table 3 lists the

Table 2. Refined Atomic Positions, Thermal Parameters, and Occupancies Obtained from Rietveld Refinement of CW-Neutron Scattering Data Obtained on Cu-SSZ-13 after Calcination

atom	x/a	y/b	z/c	U_{iso}	occ	mult./sym
T1	−0.00115	0.2282	0.10265	0.0503	1	36i
O1	0.90099	0.09891	0.12007	0.0361	1	18h
O2	0.64606	0.64606	0.5	0.0361	1	18g
O3	0.11993	0.23987	0.13098	0.0361	1	18h
O4	0	0.26283	0	0.0361	1	18f
Cu1	0	0	0.12229	0.181	0.09	6c

Table 3. Calculated Bond Lengths and Angles Obtained from Rietveld Refinement of CW-Neutron Scattering Data Obtained on Cu-SSZ-13 after Calcination

bond	distance (Å)	angle	degrees
T1−O1	1.6045	O1−T−O2	110.4
T1−O2	1.6062	O1−T−O3	108.0
T1−O3	1.6237	O1−T−O4	110.9
T1−O4	1.5852	O2−T−O3	107.2
T1−O (avg)	1.6049	O2−T−O4	109.4
		O3−T−O4	110.9
Cu−O1	2.3245	O−T−O (avg)	109.46
		T −O1−T	147.8
		T−O2−T	145.9
		T−O3−T	147.1
		T−O4−T	148.4
		T−O−T (avg)	147.42

calculated bond lengths and angles for the refined atoms. The average Si−O bond distance of 1.6049 Å is in good agreement with the average Si−O distance of 1.6099 Å as reported for CHA in the IZA database.[17] Figure 3 (right) shows the unit cell structure and the position of copper in Cu-SSZ-13 as obtained from the refinements. The position of copper in the plane of the d6r of the CHA structure is in good agreement with previously reported structures of copper in CHA.[13,26]

Synchrotron-Based Combined in Situ XAFS/XRD under NH_3-SCR Conditions. *XANES at the Cu K-Edge.* In situ XANES data were collected at the Cu K-edge on Cu-SSZ-13 under calcination and SCR conditions. Figure 4a−c compares the experimental XANES spectra collected after

dx.doi.org/10.1021/jp212450d | J. Phys. Chem. C 2012, 116, 4809−4818

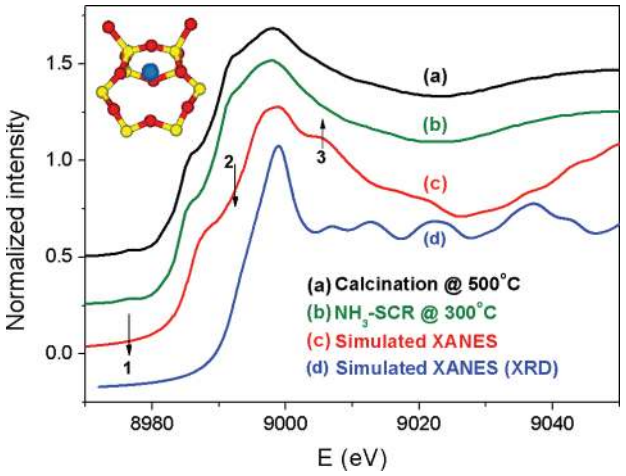

Figure 4. Cu K-edge XANES spectra of Cu-SSZ-13 (a) after calcination, (b) under NH_3-SCR conditions, (c) simulated XANES spectra calculated from a proposed structure on the basis of multiple scattering analysis of EXAFS data collected at the Cu K-edge on Cu-SSZ-13, and (d) simulated XANES based on a structure proposed from refinement of XRD data. Inset structure: local environment of Cu in the plane of the d6r of the CHA structure as per MS calculations on EXAFS data of Cu-SSZ-13 after calcination. The same local structure was used for simulation of the XANES spectrum c. In red, oxygen; in yellow, T atom; in blue, copper. Numbered arrows indicate features of interest.

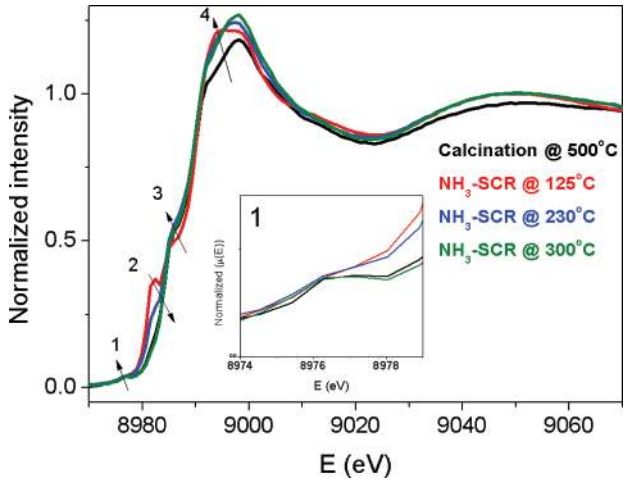

Figure 5. In situ Cu K-edge XANES spectra (normalized) of Cu-SSZ-13 after calcination (black) and under NH_3-SCR conditions at 125 °C (red), 230 °C (blue), and 300 °C (green). Features of interest are marked with numbered arrows. Inset: Magnification of the pre-edge feature (1) at 8977 eV.

calcination and under active NH_3-SCR conditions at 300 °C to a theoretical XANES spectrum of the Cu K-edge for a Cu-SSZ-13 model. The model defining the local environment of Cu in Cu-SSZ-13 was proposed on the basis multiple scattering (MS) analysis of EXAFS data collected on the sample after calcination (discussed further herein). The calculated spectrum is in very good agreement with the experimental data, confirming the validity of the proposed local environment of copper in the d6r of SSZ-13 after calcination. Features marked in the figure might appear as slight discrepancies but are easily explained. Feature 1 is absent in the calculated spectrum because the pre-edge region is not calculated during the simulations, hence emphasizing more on the edge region (that is more sensitive to the local Cu environment). Features 2 and 3 are attributed to limitations of using Density Functional Theory (DFT), due to the size of the system and the cage structure of the system itself. Nonetheless, the close match of all three presented spectra gives the first indication that the previously proposed structural model stands to be true even under active SCR reaction conditions at 300 °C. As a comparison, a second XANES spectrum (Figure 4d) was calculated based on the structure obtained from the Rietveld refinement of XRD data collected on Cu-SSZ-13. The difference between this and the structure obtained from EXAFS is that for the former, copper is found in the center of the d6r, while for the latter, the copper was found slightly distorted away from the center of the d6r. As clearly seen, a very slight movement of the absorbing atom already results in a very different calculated spectrum. The comparison serves to demonstrate the extreme sensitivity of such calculations toward the local structure it is based on.

Figure 5 compares the in situ XANES spectra measured after calcination and under SCR conditions at 125, 230, and 300 °C. Distinct pre-edge features are marked with numbered arrows. The pre-edge feature marked 1 appears at 8976 eV and has been magnified in the Figure 5 inset for clarity. This low intensity pre-edge feature has been assigned to a dipole forbidden 1s → 3d transition in planar Cu(II) complexes.[10,20,21] Cu(I) complexes do not have this transition owing to the filled d^{10} orbital, and hence, it can be used as a fingerprint for the presence of a Cu(II) system. A distinct trend can be seen in the intensity of this pre-edge feature over the different temperatures. While there is a complete overlap in position and intensity of this feature for the spectra collected after calcination and at 300 °C, the feature seems to be much weaker for the measurements taken at 125 and 230 °C, indicating a possible drop in oxidation state of copper. However, studies have also shown the intensity of the transition to depend on the coordination geometry around the absorbing atom.[27−29] Therefore, the possibility of a Cu(II) system cannot be completely ruled out.

The second pre-edge feature at 8982 eV (marked 2) is observed in the measurement taken at 125 °C under SCR conditions and appears as a shoulder at the same position for the measurement taken at 230 °C. Linear Cu(I) complexes are known to have a distinct pre-edge at ∼8982 eV similar to that seen in the spectra collected at 125 °C, owing to a transition from a 1s orbital to a double degenerate $4p_{xy}$ orbital.[30] However, given the structural environment of copper in the d6r of the CHA structure, a linear copper complex is unlikely to form. Pre-edge feature 3 appears at the absorption threshold (∼8986 eV) and is seen in all four spectra although there is a slight difference in the intensity for the spectrum measured at 125 °C. This particular feature has been seen in the past for similar copper zeolite systems and can be assigned to a Cu(II) 1s → $4p_z$ + ligand-Cu(II) change transfer (CT) excitation very similar to that seen in $Cu(OH)_2$ with the Cu in a planar geometry.[25] Finally, feature 4 at 8994 eV is only seen in the spectrum measured at 125 °C under SCR conditions. Although the contribution of this feature is not very clear, it has been observed in the past for copper in a square planar amine environment.[31,32] Chaboy et al. were able to explain this contribution by using two final state configurations of $3d^9$ and $d^{10}L$ (L = ligand hole) for the absorber atom.[33] Although not conclusive, a comparison of the XANES pre-edge features does give a qualitative description of the local environment around

dx.doi.org/10.1021/jp212450d | J. Phys. Chem. C 2012, 116, 4809−4818

the absorber atom. The absence of pre-edge features below 8985 eV (apart from the pre-edge at 8976 eV) in the spectrum after calcination and at 300 °C under SCR conditions suggest the presence of only Cu(II) under these conditions. The good agreement between the simulated spectrum (Figure 4) and those measured after calcination and under active conditions (300 °C), support the proposed position of copper in the d6r, even under active reaction conditions. Slight differences are seen at lower temperatures and will be discussed further in comparison with the EXAFS analysis.

In Situ Extended X-ray Absorption Fine Structure (EXAFS) Analysis. The results obtained from k^3-weighted EXAFS data analysis of Cu-SSZ-13 after calcination and under reaction conditions are summarized in Table 4. Figure 6 illustrates the

Table 4. Parameters Obtained from Analysis of Cu K-Edge k^3-Weighted EXAFS Data of Cu-SSZ-13 after Calcination and under Reaction Conditions at Different Temperatures[a]

temperature	shells	r (Å)	N	$2\sigma^2$ (Å^2)
after calcination	Cu−O	1.95	3	0.007
	Cu−Si	2.20	2	0.037
	Cu−O	2.93	1	0.008
	Cu−O	3.32	2	0.016
	Cu−Si	3.10	2	0.036
	Cu−O	3.32	2	0.016
	Cu−O	3.68	2	0.025
	Cu−Cu	3.76	1	0.017
	Cu−Si	4.08	2	0.032
	Cu−Si	4.16	2	0.036
	Cu−O	4.22	1	0.040
		R = 12.91%; E_f = 1.28		
125 °C	Cu−O	1.98	3	0.018
	Cu−N	2.57	1	0.032
		R = 23.95%; E_f = −6.33		
230 °C	Cu−O	1.96	3	0.015
		R = 26.55%; E_f = −4.89		
300 °C	Cu−O	1.94	3	0.014
		R = 26.90%;E_f = −3.77		

[a] r = averaged distance over 1 shell; N = coordination number; σ = Debye−Waller factor; R = statistical goodness of fit factor; E_f = Fermi energy (edge position).

experimental data and simulated fits of the k^3-weighted EXAFS data and the corresponding Fourier transforms collected after calcination and under SCR reaction conditions at 125 °C. Using the model previously proposed by us,[14] with Cu^{2+} ions present in the plane and slightly distorted from the center of the six-membered ring (analogous to Figure 4, inset), multiple scattering calculations were performed on the EXAFS data obtained after calcination. The nearest neighbor (Cu−O) bond distance of 1.95 Å and coordination number of 3 obtained from the fit after calcination are in good agreement with previously reported data by us on Cu-SSZ-13 after calcination[14] (3 oxygen atoms at 1.93 Å), thus giving the first indication of similarities in both Cu-SSZ-13 samples. As previously seen, 2 Si atoms were found at a distance of 2.20 Å in the second shell. The first difference in the presented data and that reported earlier appears in the distance to the fourth oxygen (also part of the d6r) around the absorbing copper. The Cu−O distance as reported previously was found to be 3.13 Å, while in this case, it is found to be 2.93 Å. There can be a 2-fold explanation for this: (a) the data were collected in two different collection modes (quick-XAFS vs scanning XAFS), and (b) the parent SSZ-13 materials possessed different Si/Al ratios (∼14 for the previous and ∼18 reported herein) resulting in slightly different framework compositions and hence different bond distances. Another interesting feature worth noting from the MS calculations is again the presence of a second copper at a distance of 3.76 Å.[14] Although, initially this might indicate the possible presence of dinuclear copper species, a possible explanation is obtained upon comparison with crystallographic data. As suggested by Fickel et al.[13] and as also discussed further herein, copper lies in a special position in the d6r of the CHA framework with a mirror site on the opposite face of the d6r. The distance between the two planes of the d6r in CHA comes out to be close to ∼3.8 Å, suggesting that the second copper seen in EXAFS in this case could possibly be the copper occupying the mirror site of the d6r. Considering the high Si/Al ratio, it would be statistically difficult to confirm the presence of Cu at both mirror sites. However, the inclusion of an additional Cu appeared to result in a slightly better fit for the EXAFS model.

Using the same aforementioned model, EXAFS data under SCR reaction conditions were analyzed considering only single scattering events. Figure 7 compares the FTs for the k^3-weighted EXAFS data collected under reaction conditions at 125, 230, and 300 °C. The EXAFS data under SCR conditions suggest one significant change in the local environment around the absorbing copper. As evident from the presented data in Table 4, three neighboring oxygens are consistently found at a distance of ∼1.95 Å throughout the course of the reaction as also seen after calcination. At 125 °C, this Cu−O contribution becomes slightly weaker, following a Cu−N interaction, a contribution seen at a radial distance of ∼2.57 Å as pointed out in the corresponding FTs in Figure 7 (blue arrow). The Cu−N interaction is seen to become weaker or disappear at higher temperatures. This observation is complementary to the XANES, which suggested a change in the coordination geometry around the absorbing copper at 125 and 230 °C. The change was very prominent at 125 °C and the spectra measured at 230 °C appeared as a transition of the electronic environment moving from 125 to 300 °C. Upon moving to the SCR active temperature (i.e., 300 °C), the local environment appears to be much more comparable to that seen after calcination, complementary to the XANES. The increase in the thermal contribution is reflected in the increasing Debye−Waller factors (0.007 Å^2 → 0.014 Å^2 compared after calcination to active SCR conditions at 300 °C. Nonetheless, the Cu−O distances drop back closer to the initial value after calcination suggesting a shift back to the original state of the site.

Rationalizing the XAFS Data. Combining the information obtained from both XANES and EXAFS analysis, it is reasonable to suggest a distorting environment of the copper and of the d6r unit of the zeolite framework over the course of the reaction. At lower temperatures discussed herein, changes are observed in the coordination geometry of the copper, concurrent with the appearance of a Cu−N interaction in the EXAFS. In the SCR reaction, there are two different N-containing reactants, namely, NO and NH_3. In the XANES collected at 125 °C, a clear split in the absorption line was observed, leading to two contributions at 8994 and 8998 eV. As discussed earlier, this observation correlates to a copper-amine type environment.[31−33] Additionally, NH_3, being a stronger nucleophile (due to the presence of a lone pair), is more likely to interact with the copper as compared to NO interacting with

dx.doi.org/10.1021/jp212450d | J. Phys. Chem. C 2012, 116, 4809−4818

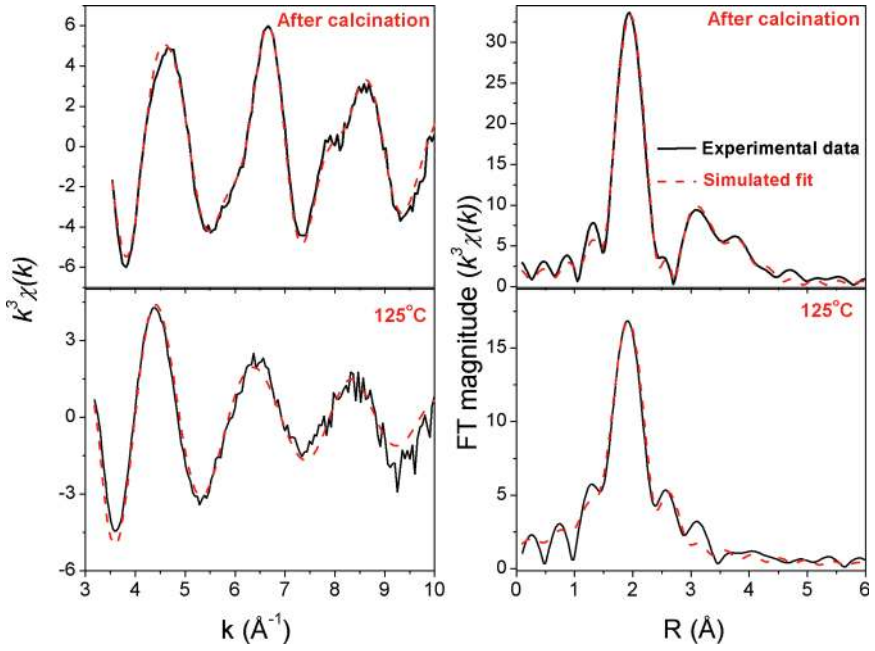

Figure 6. In situ Cu K-edge k^3-weighted EXAFS data (left) and corresponding Fourier transforms of the k^3 data (right) collected on Cu-SSZ-13 after calcination and at 125 °C under NH_3-SCR conditions. Black solid lines represent experimental data and red dashed lines represent the simulated fits.

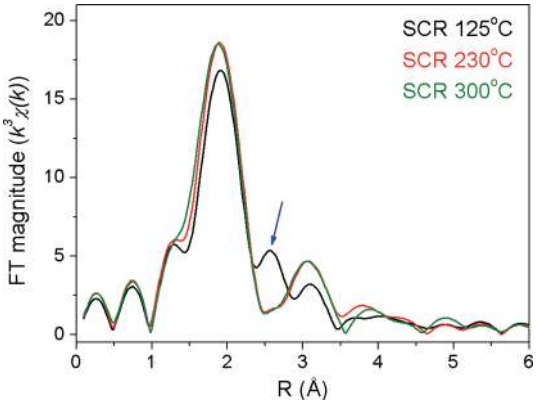

Figure 7. Comparison of the Fourier transforms of k^3-weighted EXAFS data collected at the Cu K-edge on Cu-SSZ-13 under NH_3-SCR conditions (125, 230, and 300 °C). The blue arrow indicates a contribution observed as a result of a direct Cu-NH_3 interaction, which becomes significantly weaker at higher temperatures.

the copper. Finally, coordination of linear molecules with an absorbing metal is known to be reflected in the EXAFS-FTs in the form of a significant amplitude enhancement due to multiple scattering effects. This was observed, for example with absorbing linear acetonitrile in a Co-ALPO system.[34] NO, being a linear molecule, would exhibit a similar behavior, i.e., the contribution from the oxygen of NO would be significantly enhanced in the FT. However, the particular contribution in question (expected at ~3 Å) shows no significant enhancement in the EXAFS-FT as seen from Figure 7. Given the considerations, it is plausible to propose that at lower and less active temperatures under SCR conditions, there is a direct interaction of the active site with NH_3.

Given the direct interaction of Cu with NH_3 at lower temperatures, further insight can be obtained on the slight differences seen in the XANES spectra collected at the lower temperatures. A weak 1s → 3d transition at 8977 eV coupled with the transition at 8982 eV suggested a changing environment for the absorbing copper. A drop in oxidation state of the absorbing copper could be held accountable for the changing spectra as seen in some past studies.[12] However, in the EXAFS fits performed by us, no changes were observed in the bond distances for the first or second shell after calcination and at 125 °C, trimming down the possibility of a reduction process under these conditions. In a UV−vis DRS study of the interaction of ammonia with Cu^{2+} in zeolite Y, Delabie et al. found a shift in the position of the Cu^{2+} d−d band to higher wavenumbers upon adsorbing ammonia at room temperature, a phenomenon that was found to be reversible at temperatures >250 °C.[35] However, both the intensity and position of the band did not suggest a reduction of the copper present in the system. Zeolite Y and CHA, although different framework types, are made up of similar subunits including d6rs. Theoretical calculations were performed in the same study, with copper in the plane of a 6-membered ring in zeolite Y coordinated to 3 oxygens, analogous to the system presented here. Upon adsorption, the ammonia molecule was found to interact with the copper from an axial position causing a very distorting environment for both the copper and the 6-ring of the zeolite. Such strong distortions in geometry can have a striking effect on the pre-edge features of the XANES spectra. The additional features observed in the XANES hence could be accounted for by this change in local coordination geometry rather than a redox behavior effect. The phenomenon is reversible at higher temperatures as the Cu-NH_3 interaction becomes weak. Figure 8 illustrates the proposed changing coordination geometry for copper during the reaction, which results in the changing features observed in the XANES and the additional contributions observed from the EXAFS analysis under SCR conditions. At lower temperatures, there is a very strong interaction of the active site with NH_3, causing a change from a square planar arrangement to a distorted tetrahedral environment. This conformational change could be related to an ammonia blocking effect as seen in the past from catalytic

dx.doi.org/10.1021/jp212450d | J. Phys. Chem. C 2012, 116, 4809−4818

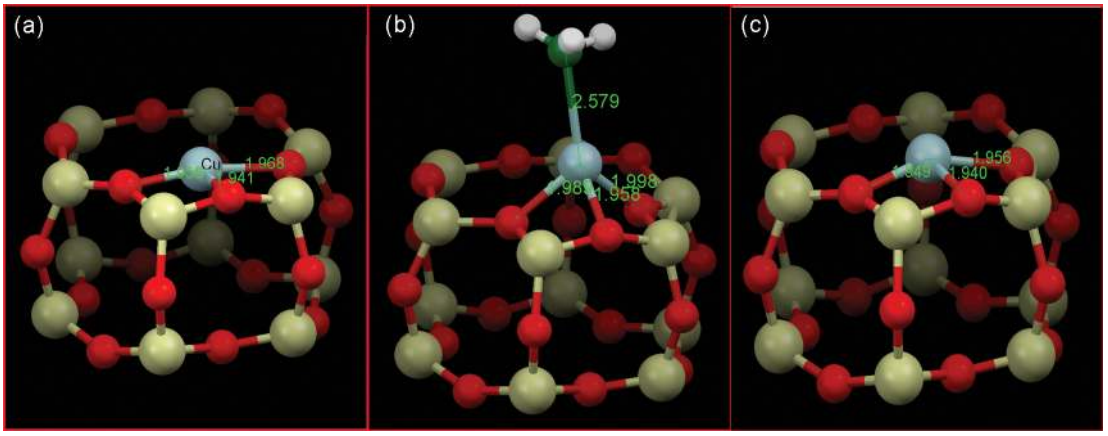

Figure 8. Illustrations of the local copper environment in d6r subunit of CHA. (a) Local structure after calcination with copper on the plane and slightly distorted from the center of the d6r subunit of CHA; (b) interaction with NH_3 at ~125 °C under SCR conditions resulting in a coordination geometry change; (c) under SCR conditions above 250 °C. The local environment is obtained from EXAFS fits using an initial model proposed from the refinement of the corresponding diffraction data collected at the different temperatures.

activity tests at lower temperatures.[36,37] Nonetheless, there is no indication of the migration of the copper away from the d6r unit of the zeolite, especially given the comparable XANES and EXAFS spectra obtained after calcination and under SCR conditions at 300 °C. The lattice oxygens in the zeolite, although strained, maintain their coordination with the copper ion, causing the relaxation back to the square planar arrangement at higher temperatures, concurrent with the maximum activity exhibited by the system.

Rietveld Refinement of in Situ XRD Data. Figure 9 shows the observed, calculated, and difference pattern obtained from

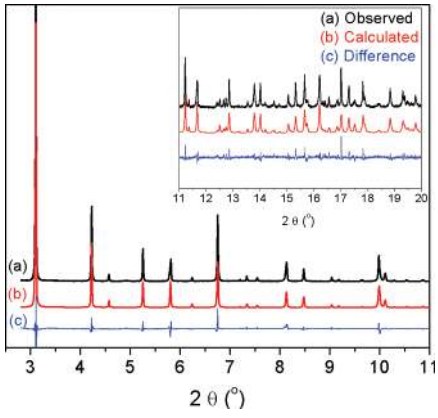

Figure 9. Observed (black), calculated (red), and difference (blue) patterns obtained from the Rietveld refinement of X-ray diffraction collected on Cu-SSZ-13 under SCR reaction conditions at 300 °C. The pattern has been magnified for clarification (inset) between 11 and 20 2θ. X-ray synchrotron radiation λ = 0.50117 Å; space group, $R\bar{3}m$; refined unit cell, $a = b$ = 13.530 Å, c = 14.792 Å; vol, 2345.2 Å^3.

the Rietveld refinement of XRD data on Cu-SSZ-13 under SCR conditions at 300 °C with the corresponding experimental and refinement details tabulated in Table 5. Table 6 and 7 compare the bond distances and angles obtained from the Rietveld refinement of powder X-ray diffraction measurements on Cu-SSZ-13 after calcination and under SCR conditions at 80, 180, and 300 °C. As seen, the average Si−O bond length after calcination and under SCR conditions (1.60 Å) are in close agreement with that obtained from the Neutron diffraction

Table 5. Experimental Parameters and Goodness of Fit Factors for Rietveld Refinement of XRD Data Obtained on Cu-SSZ-13 after Calcination and under Active Reaction Conditions (300 °C)

			value	
exptl parameter	value	parameter	after calcination	SCR 300 °C
wavelength (λ)	0.5011 Å	χ^2	3.4	3.1
scanned region (2θ)	2−25	R_{wp}	24.9 (18.2)	24.2 (17.1)
refinement region (2θ)	2.8−20	R_p	19.1 (13.4)	19.2 (12.5)
		R_{exp}	12.98	13.53 (9.53)

Table 6. Selected Bond Distances of Interest for Cu-SSZ-13 Obtained from Rietveld Refinement of XRD Data after Calcination and under NH_3-SCR Reaction Conditions (at 80, 180, and 300 °C)

	distance (Å)			
bond	after calcination	SCR 80 °C	SCR 180 °C	SCR 300 °C
T1−O1	1.6166	1.6143	1.6199	1.6215
T1−O2	1.6228	1.5995	1.6007	1.5974
T1−O3	1.6122	1.6078	1.6102	1.6135
T1−O4	1.5847	1.5925	1.5869	1.5985
T1−O (avg)	1.609	1.6035	1.6044	1.6044
Cu−O1	2.329			2.3427

analysis (Table 2) and those reported in the literature.[13,17] The averaged O−T−O bond angle (109.3° after calcination and 109.4° under SCR conditions) are also in agreement with a tetrahedral coordination. Refinement of the powder pattern collected after calcination showed copper to be present in the d6r unit of the CHA structure analogous to the results from neutron diffraction (Figure S3, Supporting Information). The copper was found to be in a planar environment coordinated to three (symmetrically equivalent) oxygens at a distance of 2.32 Å. The obvious difference in the Cu−O bond distance as obtained from EXAFS (1.95 Å) and as obtained from XRD (2.32 Å) is inherent in the probing order of each technique itself. While EXAFS probes local environments and hence can be sensitive to very local changes such as a slight movement away from the center of the d6r, diffraction, being a long-range

dx.doi.org/10.1021/jp212450d | J. Phys. Chem. C 2012, 116, 4809−4818

Table 7. Selected Bond Angles of Interest for Cu-SSZ-13 Obtained from Rietveld Refinement of XRD Data after Calcination and under NH_3-SCR Reaction Conditions (at 80, 180, and 300 °C)

	degrees			
angle	after calcination	SCR 80 °C	SCR 180 °C	SCR 300 °C
O1−T−O2	107.7	108.1	107.4	106.1
O1−T−O3	110.2	109.0	108.4	107.2
O1−T−O4	113.5	110.1	110.3	113.9
O2−T−O3	106.0	107.9	107.7	108.5
O2−T−O4	107.9	109.2	109.6	107.8
O3−T−O4	111.0	112.1	113.0	113.0
O−T−O (avg)	109.3	109.4	109.4	109.4
T−O1−T	146.0	149.3	149.5	148.9
T−O2−T	148.8	149.8	149.3	152.8
T−O3−T	147.3	147.3	146.6	147.6
T−O4−T	142.4	146.9	147.2	141.1
T−O−T (avg)	147.4	148.3	148.15	146.9

order technique is limited in observing local changes due to symmetry rules that define a refinement. Hence, shifting the copper position away from the center of the d6r results in a loss of symmetry, and hence, a poor fit as was also observed by Fickel et al.[13] Upon moving to the SCR conditions, this phenomenon was seen to have a stronger effect on the obtained results. First, slight changes were observed in the bond distances and angles between the T and O atoms of the zeolite itself. Second, under SCR conditions, at 80 and 180 °C, modeling the Cu in the plane of the d6r consistently resulted in the copper moving away from the d6r during the course of the refinement. To further account for the movement away from the d6r, four alternative cationic positions for copper in the CHA structure were also modeled. These positions were (a) in the center of the 8-membered ring window; (b) in the center of the ellipsoidal cavity; (c) in the middle of the d6r unit (between the two 6-rings); and (d) in the center of the 4-membered rings connecting the d6r units (Figure S4, Supporting Information). However, the refinements were seen to worsen in each case whether the alternative site was modeled alone or in combination with the already suggested site in the d6r. The XANES and EXAFS results at these temperatures already gave a clear indication of a change in the co-ordination environment around the absorbing copper atom. Given the results, this was attributed to the copper coordinating with an NH_3 molecule at an axial position, leading to a change from a square-planar environment to a distorted tetrahedral-type environment at 125 °C. The highly distorted environment resulting from the Cu-NH_3 interaction coupled with framework distortions of the zeolite could possibly provide an explanation for not being able to account for a precise position of the copper from the refinements performed under these conditions.

Whether the blocking interaction of NH_3 with the active site is a required activation step in the catalytic cycle cannot be confirmed with the performed studies. Studies performed on Cu-zeolite systems in the past have considered different reaction intermediates. In some cases, the importance of Cu-amine type species coupled to an interaction with NO has been stressed as a required active phase for the SCR reaction,[38,39] while others have proposed formation of a N_xO_y-metal species, which further reacts with NH_3.[40] Delahay and co-workers have also suggested that one NH_3 molecule remains permanently bonded to the Cu (in Cu-FAU) over the course of the SCR reaction and that the reaction proceeds via a redox cycle involving Cu-NH_3 interaction, subsequent oxidation, and formation of Cu-N_xO_y species and their further reaction with NH_3 to give N_2.[41]

Furthermore, as was seen with the XAS data, under active SCR conditions at 300 °C, the copper environment was comparable to that seen after calcination. Figure S5 of the Supporting Information compares the structural position of copper after calcination and under active SCR conditions (300 °C) as obtained from Rietveld refinement of the corresponding powder patterns. Under SCR-active conditions, the copper maintains its position as an isolated ion in the d6r of the CHA structure. There are slight changes in the bond distances and angles around the copper and of the zeolite framework itself, as already suggested by EXAFS analysis. The changes are indicative of a flexible environment of the active site under reaction conditions. Nonetheless, the overall position of the isolated copper from the d6r unit of the zeolite is not altered and this predominant position acts as the active sites under reaction conditions for the SCR process (Table 8).

Table 8. Refined Atomic Positions, Thermal Parameters, and Occupancies for Cu-SSZ-13 Obtained from Rietveld Refinement of XRD Data Obtained under Active SCR Conditions (300 °C)[a]

atom	x/a	y/b	z/c	U_{iso}	occ	mult./sym
T1	0.00010	0.22905	0.10191	0.02115	1	36i
O1	0.90070	0.09920	0.12305	0.03756	1	18h
O2	0.64226	0.64226	0.5	0.03756	1	18g
O3	0.11981	0.23964	0.13120	0.03756	1	18h
O4	0	0.26834	0	0.03756	1	18f
Cu1	0	0	0.14498	0.03675	0.05	6c

[a] U_c: $a = b = 13.5303$; $c = 14.7927$; vol, 2345.2647.

CONCLUSIONS

Cu-SSZ-13 catalysts are very active in the NH_3-SCR of NO_x gases and show a high selectivity toward the desired N_2 formation. In this study, we examined the origin of the SCR activity of Cu-SSZ-13 zeolite (CHA framework) considering the active site location, coordination geometry, and redox functionality of the active component (Cu) using a combination of laboratory and synchrotron-based techniques. The following conclusions can be drawn from this study:

(1) Isolated mononuclear Cu^{2+} cations located on the plane and slightly distorted from the center of the d6r subunits of SSZ-13 were identified as active sites of the catalyst after calcination and under active SCR reaction conditions at 300 °C.

(2) A conformational change (from a square planar to a distorted tetrahedral type environment) as a result of a direct interaction of NH_3 with copper as seen at lower temperatures (125 °C) correlates to a lower catalytic activity of the system at these temperatures. This change in the coordination geometry was reversible at higher temperatures and was concurrent with observing maximum catalytic activity.

(3) The importance of this blocking interaction in the catalytic cycle is challenging to address given the scope of

dx.doi.org/10.1021/jp212450d | J. Phys. Chem. C 2012, 116, 4809−4818

this study. Combined spectroscopic studies focused within these (lower) temperature ranges and with altering reactant gas concentrations could reveal further valuable information on maximizing activity under these conditions.

■ ASSOCIATED CONTENT

Supporting Information

Equations used for calculating the conversion of NOx and the selectivity toward outlet gases; experimental setup used to study catalytic activity under plug flow conditions in the laboratory compared to the experimental setup used to perform synchrotron-based combined in situ XAS/XRD on Cu-SSZ-13 catalysts under reaction conditions; UV−vis-NIR diffuse reflectance spectra and powder X-ray diffraction patterns of Cu-SSZ-13 before and after NH_3-SCR; Rietveld refinement of X-ray diffraction collected on Cu-SSZ-13 after calcination; different modeled crystallographic positions of copper in the CHA structure to account for low temperature (80 and 180 °C) position of copper in the CHA structure; fragment of the d6r subunit illustrating the crystallographic position of copper in the d6r of SSZ-13 as obtained from Rietveld refinement of X-ray diffraction data collected on Cu-SSZ-13 after calcination and under SCR conditions at 300 °C. This material is available free of charge via the Internet at http://pubs.acs.org.

■ AUTHOR INFORMATION

Notes

The authors declare no competing financial interest.

■ ACKNOWLEDGMENTS

This research was carried out under project number M23.7.08301 in the framework of the Research Program of the Materials innovation institute M2i (www.m2i.nl). We would like to thank Sachem Inc. for kindly providing the template (ZeoGen 2825) used in the synthesis of SSZ-13. For the XANES simulations, the work was granted access to the HPC resources of IDRIS under the allocation 2011-1202 made by GENCI (Grand Equipment National de Calcul Intensif). Inés Dácil González-Jiménez (Utrecht University) is thanked for helping with experiments at SNBL, ESRF. ESRF is thanked for funding the beamtime to perform combined XAS/XRD measurements. Matthew G. O'Brien (Utrecht University) and David Wragg (Oslo University) are thanked for advice on Rietveld refinements.

■ REFERENCES

(1) EU Commission.. *Official Journal of the European Union* **2011**, 1−168.
(2) Emission Standards USA: Heavy Duty Truck and Bus Engines. www.dieselnet.com.
(3) Burch, R. *Catal. Rev. Sci. Eng.* **2004**, *46*, 271.
(4) Brandenberger, S.; Krocher, O.; Tissler, A.; Althoff, R.; Kröcher, O. *Catal. Rev. Sci. Eng.* **2008**, *50*, 492.
(5) Bull, I.; Boorse, R. S.; Jaglowski, W. M.; Boorse, S.; Jaglowski, W. M.; Koermer, G. S.; Moini, A.; Patchett, J. A.XenW.;BurkP. Dettling, J. C.; Caudle, M. T. Copper CHA zeolite catalysts. World Patent 106519, 2008.
(6) Kwak, J. H.; Tonkyn, R. G.; Kim, D. H.; Szanyi, J.; Peden, C. H. F. *J. Catal.* **2010**, *275*, 187.
(7) Moretti, G.; Ferraris, G.; Fierro, G.; Jacono, M.; Morpurgo, S.; Faticanti, M. *J. Catal.* **2005**, *232*, 476.
(8) Centi, G.; Perathoner, S. *Appl. Catal., A* **1995**, *132*, 179.
(9) Dzwigaj, S.; Janas, J.; Gurgul, J.; Socha, R.; Shishido, T.; Che, M. *Appl. Catal., B* **2009**, *85*, 131.
(10) Praliaud, H. *Appl. Catal., B* **1998**, *16*, 359.
(11) Mathisen, K.; Nicholson, D. G.; Stockenhuber, M. *Phys. Chem. Chem. Phys.* **2009**, *11*, 5476.
(12) Kispersky, V. F.; Kropf, A. J.; Ribeiro, F. H.; Miller, J. T. *Phys. Chem. Chem. Phys.* **2012**, *14*, 2229.
(13) Fickel, D. W.; Lobo, R. F. *J. Phys. Chem. C* **2010**, *114*, 1633.
(14) Korhonen, S. T.; Fickel, D. W.; Lobo, R. F.; Weckhuysen, B. M.; Beale, A. M. *Chem. Commun.* **2011**, *47*, 800.
(15) Larson, A. C.; Von Dreele, R. B. *General Structure Analysis System (GSAS)* **2000**, *748*, 86.
(16) Toby, B. H. *J. Appl. Crystallogr.* **2001**, *34*, 210.
(17) Database of Zeolite Structures. www.iza-structure.org/databases.
(18) Giannozzi, P.; Baroni, S.; Bonini, N.; Calandra, M.; Car, R.; Cavazzoni, C.; Ceresoli, D.; Chiarotti, G. L.; Cococcioni, M.; Dabo, I.; Dal Corso, A.; de Gironcoli, S.; Fabris, S.; Fratesi, G.; Gebauer, R.; Gerstmann, U.; Gougoussis, C.; Kokalj, A.; Lazzeri, M.; Martin-Samos, L.; Marzari, N.; Mauri, F.; Mazzarello, R.; Paolini, S.; Pasquarello, A.; Paulatto, L.; Sbraccia, C.; Scandolo, S.; Sclauzero, G.; Seitsonen, A. P.; Smogunov, A.; Umari, P.; Wentzcovitch, R. M. *J. Phys.: Condens. Matter* **2009**, *21*, 395502.
(19) Gougoussis, C.; Calandra, M.; Seitsonen, A.; Brouder, C.; Shukla, A.; Mauri, F. *Phys. Rev. B* **2009**, *79*, 045118.
(20) Gougoussis, C.; Calandra, M.; Seitsonen, A.; Mauri, F. *Phys. Rev. B* **2009**, *80*, 075102.
(21) Taillefumier, M.; Cabaret, D.; Flank, A.-M.; Mauri, F. *Phys. Rev. B* **2002**, *66*, 195107.
(22) Binsted, N. *EXCURV*, CCLRC Daresbury Laboratory Computer Program, 1998.
(23) Rodriguez-Carvajal, J. *Phys. C* **1993**, *212*, 259.
(24) Rodriguez-Carvajal, J. *IUCr Newsletter* **1998**, 35.
(25) Groothaert, M. H.; VanBokhoven, J. A.; Battiston, A. A.; Weckhuysen, B. M.; Schoonheydt, R. A. *J. Am. Chem. Soc.* **2003**, *125*, 7629.
(26) Gualtieri, A. F.; Passaglia, E. *Eur. J. Mineral.* **2006**, *18*, 351.
(27) Kau, L. S.; Spira-Solomon, D. J.; Penner-Hahn, J. E.; Hodgson, K. O.; Solomon, E. I. *J. Am. Chem. Soc.* **1987**, *109*, 6433.
(28) Sano, M.; Komorita, S.; Yamatera, H. *Inorg. Chem.* **1992**, *31*, 459.
(29) Kervinen, K.; Bruijnincx, P. C. A.; Beale, A. M.; Mesu, J. G.; van Koten, G.; Klein Gebbink, R. J. M.; Weckhuysen, B. M. *J. Am. Chem. Soc.* **2006**, *128*, 3208.
(30) Durá, O.; Boada, R.; Rivera-Calzada, A.; León, C.; Bauer, E.; de la Torre, M.; Chaboy, J. *Phys. Rev. B* **2011**, *83*, 045202.
(31) Mesu, J. G.; Visser, T.; Beale, A. M.; Soulimani, F.; Weckhuysen, B. M. *Chem.—Eur. J.* **2006**, *12*, 7167.
(32) Frank, P.; Benfatto, M.; Hedman, B.; Hodgson, K. O. *Inorg. Chem.* **2008**, *47*, 4126.
(33) Chaboy, J.; Muñoz-Páez, A.; Carrera, F.; Merkling, P.; Marcos, E. *Phys. Rev. B* **2005**, *71*, 134208.
(34) Barrett, P. A.; Sankar, G.; Jones, R. H.; Catlow, C. R. A.; Thomas, J. M. *J. Phys. Chem. B* **1997**, *5647*, 9555.
(35) Delabie, A.; Pierloot, K.; Groothaert, M. H.; Weckhuysen, B. M.; Schoonheydt, R. A. *Microporous Mesoporous Mater.* **2000**, *37*, 209.
(36) Grossale, A.; Nova, I.; Tronconi, E. *J. Catal.* **2009**, *265*, 141.
(37) Grossale, A.; Nova, I.; Tronconi, E.; Chatterjee, D.; Weibel, M. *Top. Catal.* **2009**, *52*, 1837−1841.
(38) Eun, Y. C.; In-Sik, N.; Young, G. K.; Jong, S. C.; Jae, S. L.; Nomura, M. *J. Mol. Catal. A: Chem.* **1991**, *69*, 247.
(39) Ham, S.-W.; In-Sik, N.; Kim, Y. G. *Catal. Lett.* **1996**, *42*, 35.
(40) Mastikhin, V. M.; Filimonova, S. V. *J. Chem. Soc. Faraday Trans.* **1992**, *88*, 1473.
(41) Delahay, G.; Kieger, S.; Tanchoux, N.; Trens, P.; Coq, B. *Appl. Catal., B* **2004**, *52*, 251.